ADVANCED MATERIALS TECHNOLOGIES
www.advmattechnol.de

Knocking the Stability of Solar Cells with Fluorescent Protein Donors upon Rationalizing Design, Integration, and Mechanism

*Sanchari Chowdhury, Mattia Nieddu, Marta Patrian, David Gutiérrez-Armayor, Luca M. Cavinato, Juan Pablo Fuenzalida-Werner, Miquel García Lleó, Simone Ligi, and Rubén D. Costa**

Though photon-induced electron donor features of fluorescent proteins (FPs) in solution suggest them as excellent photosensitizers, their poor stability upon device fabrication/operation is the today's frontier. This relates to their immediate denaturation in water-free/less environments: inorganic/organic device interfaces and/or organic solvent surroundings. This study provides a fresh solution with a family of hybrid FPs, in which the peripheral carboxylic groups of archetypal FPs -superfolder green fluorescent protein (sfGFP) and mCherry- are transformed into alkoxysilane groups, enabling a straightforward integration with surprising stabilities over months in devices – arbitrary n/p-type semiconducting metal oxide/FP/organic-solvent electrolyte interfaces – attributed to the formation of an ion-silica shell around the FP. This further allowed to understand the charge injection mechanism applying steady-state/time-resolved spectroscopy on different FP-variants with key single-point aromatic amino acid mutations at the chromophore nearest, revealing the electron-donor hopping pathway via the initial loop of the strand β7. Finally, devices with state-of-the-art solar-to-energy conversion efficiencies that are stable >2,000 h under operation nicely outperform the prior-art stability of a few seconds/minutes in FP-based solar cells. Hence, this work solves the integration/stability issues which blocking the application of FP-based sensitizer, as well provides a solid understanding of their photo-induced electron transfer mechanism.

1. Introduction

Biogenic materials/compounds, such as photosynthetic light-harvesting systems, DNA, polysaccharides, and fluorescent and/or redox proteins, have always drawn the attention as a paradigm of sustainable energy materials in solar cells to meet eco-efficiency and device performance expectations.[1–6] Concerning solar-to-energy conversion efficiencies (η), the leading examples are i) bio-derived dye-sensitized solar cells (BSSCs) based on chlorophyll photosensitizer with short-circuit currents (J_{sc}) of 13.7 mA cm^{-2} and η of 4.2%,[7] ii) bio-based perovskite solar cells (BPSCs) using functionalized TiO_2 with bacteriorhodopsin protein as electron transport layer, realizing slightly enhanced device performance compared to reference devices (η>17%),[8] and iii) bio-hybrid organic solar cells (BOSC) with η of 10.88% upon enhancing the panchromatic absorption of the active layer combining the light-harvesting complex II and polymer:[6,6]-phenyl-C61-butyric acid methyl ester.[9]

Despite the above promising η values, the major concerns in bio-hybrid solar cells are i) the need for easy ways to implement biogenic materials into conventional device fabrication methodologies,[10,11] and ii) the common poor device stability caused by the quick bio-functionality loss in water-free/less environments/interfaces and working temperature/irradiation conditions, leading to the formation of dielectric materials that hamper charge separation and transport processes.[12,13] These are especially critical for biogenic photosensitizers rather than biogenic charge transport layers and/or doping agents. In detail, the most stable BPSCs refer to those implementing DNA as hole-transport material, retaining 90% of stability after a long-term air exposure,[2] as well as dopamine doped PEDOT:PSS and amino acid-doped TiO_2 transport layers –, i.e.,15% η loss after 28 days.[14,15] Likewise, best bio-DSSCs with stabilities >1,000 h were achieved using liquid and *quasi*-solid polysaccharide-based aqueous electrolytes,[16] while BOSCs bearing poly-lysine as electron transport layers showed an

S. Chowdhury, M. Nieddu, M. Patrian, D. Gutiérrez-Armayor, L. M. Cavinato, J. P. Fuenzalida-Werner, R. D. Costa
Chair of Biogenic Functional Materials
Technical University of Munich
Campus Straubing for Biotechnology and Sustainability
Schulgasse 22, 94315 Straubing, Germany
E-mail: ruben.costa@tum.de
M. G. Lleó, S. Ligi
Graphene XT s.r.l
Via d'Azeglio 15, Bologna 40 123, Italy

The ORCID identification number(s) for the author(s) of this article can be found under https://doi.org/10.1002/admt.202301968

DOI: 10.1002/admt.202301968

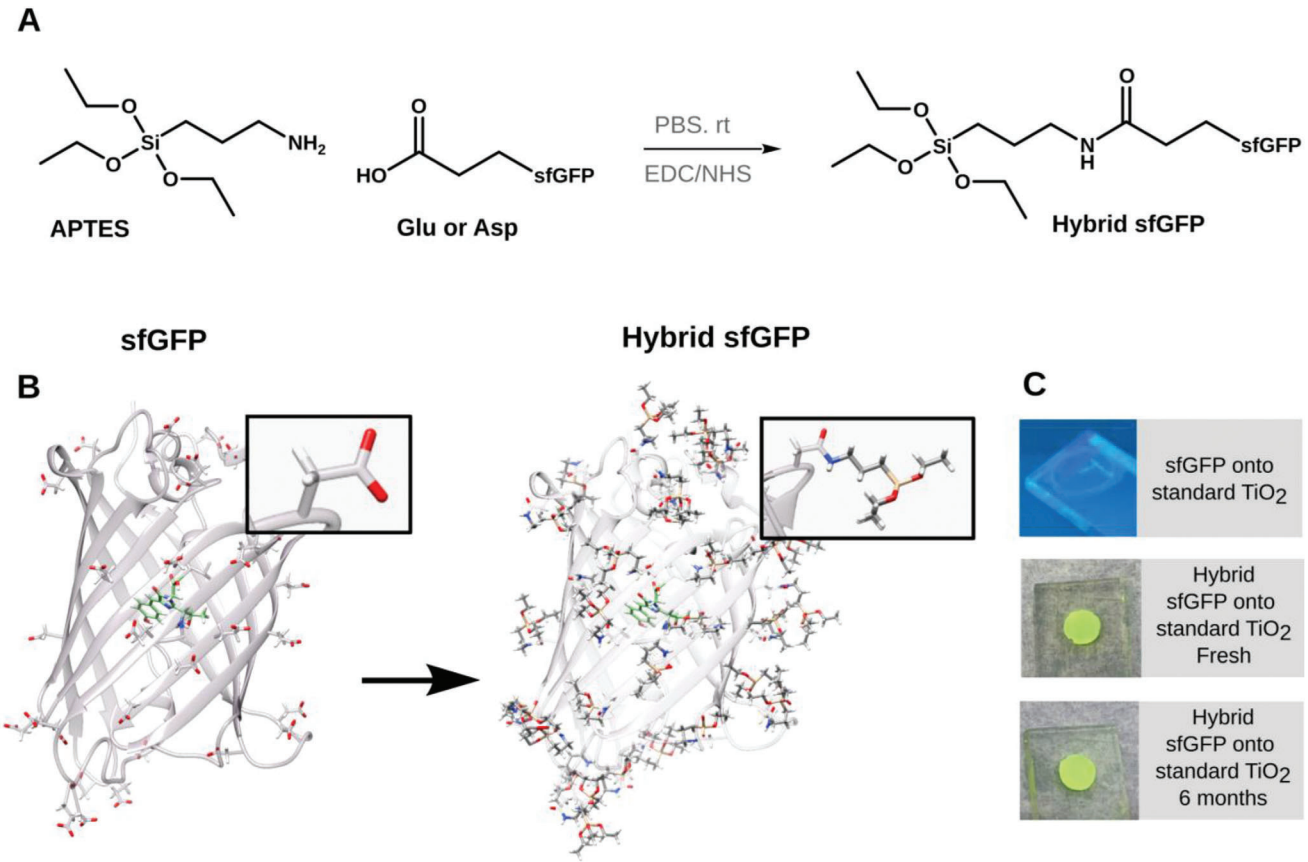

Figure 1. A,B) Concept highlighting the synthesis and C) the benefits of the hybrid FPs showing the successful sensitization and stability of standard TiO_2 electrodes.

improved η with a record stability of 20% loss after 400 h under operation.[17] In contrast, the most stable devices with bio-derived photosensitizers are bio-DSSCs with curcumin dyes featuring <200 h at η 0.18%.[18] In comparison, those integrating more complex biogenic photosensitizers, such as light-harvesting complex and/or fluorescent/redox proteins, have typically exhibited very poor stabilities ranging from seconds to minutes.[19] In particular, bio-DSSCs with protein-like photosensitizers are restricted to enhanced green fluorescent protein (eGFP), reaching average η values <0.3%,[20] and bacteriorhodopsin protein, reaching average η values <0.4%.[21] Here, the blessing and curse is the protein skeleton that shields the chromophore from the environment, maximizing its photoluminescence behavior, but it is prone to severe structural distortion upon adsorption onto the semiconducting metal oxide electrodes and under redox regeneration with organic solvent electrolytes. These lead to a quick loss of the protein functionality and, in turn, to a complicated device fabrication and very poor device stabilities that have not allowed us to understand their photon-induced electron donor/acceptor behavior in solid-state or thin-films.[22] Hence, the implementation/operation stability of protein-based photosensitizers is a major challenge in the field of bio-hybrid solar cells.

Herein, we demonstrate a fresh concept to realize this milestone with the design of a family of hybrid FPs with archetypal super folder green fluorescent proteins (sfGFP) and mCherry, in which the peripheral carboxylic groups are straightforwardly transformed into alkoxysilane groups – **Figure 1**. The advantage of this functionalization is two-fold: i) the enhancement of the FP adsorption onto arbitrary n/p-semiconducting metal oxide electrodes via alkoxysilane condensation, and ii) an excellent stabilization of the FP-electrodes over months under ambient storage and device working conditions attributed to the formation of a partial ion-silica shell around the protein surface that prevents denaturation without affecting charge injection from FP to metal oxide and the subsequent FP-electrolyte regeneration process. What is more, this allowed us to determine the exclusive electron-donor hopping mechanism of FPs applying time-resolved spectroscopy to i) sensitized p/n-type electrodes with/without dielectric interlayers along with FPs with/without proven charge transfer character –, i.e., sfGFP versus mCherry,[23] and ii) n-type electrodes with sfGFP variants with key single-point aromatic amino acid mutations at the chromophore nearest, revealing an electron-donor hopping pathway via the initial loop of the strand β−7. Finally, after optimizing device fabrication and all components –, i.e., photoanode, electrolyte, counter-electrode, these bio-DSSCs featured J_{sc} of 0.66 mA cm^{-2}, open-circuit voltage (V_{oc}) of 0.66 V, and fill factors (FF) of 0.70 that resulted in slightly enhanced η values of 0.3% compared to the prior-art of GFP-based photosensitizer.[20] What is more striking, these figures-of-merit held constant over 2,160 h, representing a significant jump compared to the most stable solar cells with biogenic photosensitizers (<200 h at 20% efficiency loss),[18] in general, and protein-based

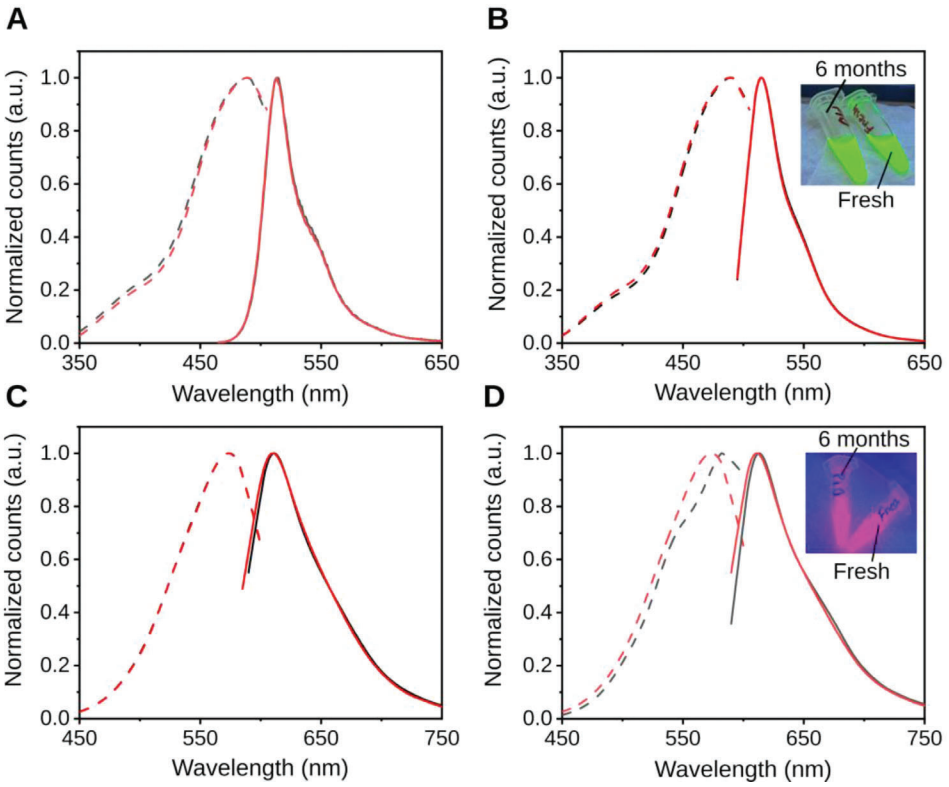

Time	τ (ns)	Φ (%)
Native sfGFP	3.09	63
Hybrid sfGFP	3.12	66
Six months	3.07	63

Time	τ (ns)	Φ (%)
Native mCherry	1.62	21
Hybrid mCherry	1.77	29
Six months	1.72	28

Figure 2. A) Excitation (dashed line) and emission (solid line) of native (black) and hybrid (red) sfGFP as well as their respective τ and ϕ figures gathered in the table. B) Excitation (dashed line) and emission (solid line) spectra of fresh (black) and 6-month old (red) aqueous solution of hybrid sfGFP as well as their respective τ and ϕ figures gathered in the table. Pictures of fresh and 6-month old solutions of hybrid sfGFP under UV lamp. C) Excitation (dashed line) and emission (solid line) of native (black) and hybrid (red) mCherry as well as their respective τ and ϕ figures gathered in the table, D) Excitation (dashed line) and emission (solid line) spectra of fresh (black) and 6-month old (red) aqueous solution of hybrid mCherry as well as their respective τ and ϕ figures gathered in the table. Pictures of fresh and 6-month old solutions of hybrid mCherry under UV lamp. *All τ fittings and ϕ gave errors <0.03 and <2% respectively.

photosensitizers (second to minutes), in particular.[20] Overall, this work provides a successful concept with a straightforward external functionalization of, in principle, any photo/redox proteins, overcoming the implementation and stability challenges in protein-based solar cells.

2. Results and Discussion

2.1. Synthesis and Characterization of Hybrid FPs

As above mentioned, the fabrication of FP-based active layers for solar cells has always faced limitations with respect to their immediate denaturation of FPs in dry films and their weak adsorption onto metal oxide electrodes despite the high number of anchoring groups at the FP surface –, i.e., carboxylic, phenol groups, etc. As an example, Figure 1 and Figure S1 (Supporting Information) depict the weak adsorption of native sfGFP onto standard transparent TiO_2 electrodes applied to DSSCs using aqueous (phosphate buffer pH ≈7.4) solutions and literature procedures of 70 °C and 4 °C for short (1 or 2 h) and long (24 and 48 h) of soaking time, respectively – see supporting information.[20,24] While these conditions can preserve protein structure with a negative surface to ensure covalent attachment onto the metal oxide electrode, the hydrophobic nature of TiO_2 prevents an efficient wettability of the electrode surface even at high temperatures.[25] Here, the most promising sensitization method was 4 °C for 24 h; though the FP uptake remains very poor – Figure S1 (Supporting Information). Indeed, these devices featured a very low η of 0.004% at 1 sun AM1.5 illumination, regardless of the type of electrolyte – Figure S1 (Supporting Information). Hence, other attaching concepts must be identified to meet high compatibility with FPs and a high affinity with metal oxide electrodes at the above aqueous conditions. Inspired by the sol-gel field,[26,27] we proposed to functionalize the peripheral carboxylic groups of native FPs with amino-alkoxysilane linkers (APTES, or (3-Aminopropyl)triethoxysilane) that should easily condensate onto the metal oxide surface electrodes enhancing FP uptake.[28,29] At first, the amidation reaction is straightforward by drop-wise adding APTES in a concentrated solution (5 mg ml^{-1}) of either sfGFP or mCherry at pH = 7 phosphate buffer under gentle stirring conditions at room temperature for 24 h– Figure 1 and supporting information. IR spectroscopy of the hybrid FP confirmed the presence of a Si-O stretching band ≈1070 cm^{-1}, while elemental analysis and mass spectroscopy suggested a functionalization of 14–17 carboxylic acid groups on both protein surfaces – Figure S2 (Supporting Information).

As shown in **Figure 2**A,C, the hybrid FPs featured a similar excitation and emission spectra to those of the native FPs, but

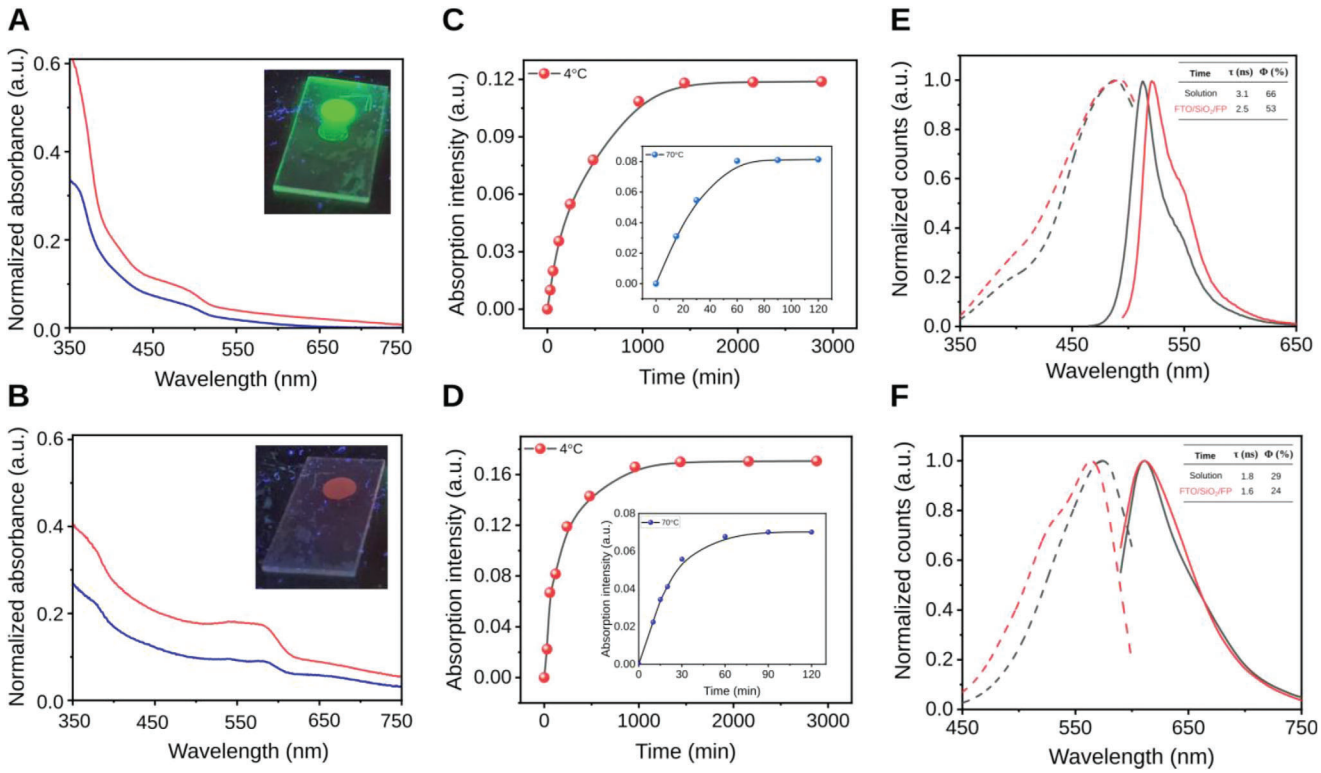

Figure 3. Exemplary UV–vis absorption spectra of FTO/TiO_2 films soaked with hybrid sfGFP A) and hybrid mCherry B) at 70 °C for 1 h (blue) and 4 °C for 24 h (red). Inset: Pictures of the sensitized FTO/TiO_2 electrodes with hybrid sfGFP and mCherry under UV lamp. C) Adsorption kinetics of hybrid-sfGFP at 4 °C and 70 °C (inset). D) Adsorption kinetics of hybrid-mCherry at 4 °C and 70 °C (inset). E) Excitation (dashed line), emission (solid line), and their respective figures-of-merit of hybrid sfGFP solution (black), FTO/SiO_2/hybrid-sfGFP (red). F) Excitation (dashed line), emission (solid line), and their respective figures-of-merit of hybrid mCherry solution (black), FTO/SiO_2/hybrid-mCherry (red). *All τ fittings and ϕ gave errors <0.03 and <2% respectively.

the excited state lifetimes (τ) and photoluminescence quantum yields (ϕ) are slightly enhanced –, i.e., τ of 3.09 ns versus 3.12 ns and 1.62 versus 1.77 ns and ϕ of 63% versus 66% and 21% versus 29% for native sfGFP and mCherry versus respective hybrid derivatives (see Table in Figure 2). Thus in both cases, the hybrid FPs might feature a more rigid β-barrel, increasing the chromophore rigidity.[30–32] In addition, the lack of emission features at the 400–470 nm region in sfGFP derivatives attests that the chromophore did not change into its neutral form upon functionalization.[30–33] Finally, the hybrid FPs are stable in aqueous media, as confirmed by the lack of sediments and changes of the above figures upon storage under ambient and dark conditions over 6 months – Figures 1 and 2B,D.

2.2. Characterization of Sensitized Electrodes with Hybrid FPs

Standard n-type TiO_2 and p-type NiO electrodes and reference SiO_2 layers were prepared onto fluorine tin-oxide (FTO) glass substrates following the reports elsewhere – see Supporting Information.[34,35] At first, adsorption kinetics assays were performed monitoring the absorption features of the films immersed in the hybrid FP aqueous solutions over time following the above best conditions. In stark contrast to the native reference FPs – Figure 1 and Figure S1 (Supporting Information) – the sensitized electrodes feature a significantly improved FP uptake, as highlighted by their colorful aspect, while the absorption intensity saturates at 24 h, suggesting a full coverage of the electrode – **Figure** 3A–D.

Further corroboration about the FP stability upon adsorption onto the electrodes came from photoluminescence assays. In reference FTO/SiO_2/FPs films, the shape of the excitation and emission spectra are similar to those in solution – Figure 3E,F – showing a slightly red-shifted emission maxima wavelength (*ca.* 10 nm) and a slightly higher intensity of the neutral form. In addition, both hybrid FPs showed faintly shorted τ and reduced ϕ values compared to those in solution –, i.e., 2.5 ns and 53% versus 3.1 ns and 66% for FTO/SiO_2/hybrid sfGFP versus hybrid sfGFP solution; 1.6 ns and 24% versus 1.8 ns and 29% for FTO/SiO_2/hybrid mCherry versus hybrid mCherry solution. These findings suggest a partial distortion of the protein barrel structure upon adsorption onto the SiO_2 layer,[30–33] likely due to the autocatalytic condensation of the alkoxysilane groups forming an ion silica shell around the FP structure.[36]

In stark contrast to the FTO/SiO_2/FPs reference films, the τ and ϕ values of the hybrid sfGFP are strongly reduced to 1.9 ns and 39% upon adsorption onto the FTO/TiO_2 electrodes – **Figure** 4A, while those with hybrid mCherry electrodes hold fairly constant –, i.e., 1.5 ns and 22% – Figure 4C. This could be related to either a severe distortion of the hybrid sfGFP upon

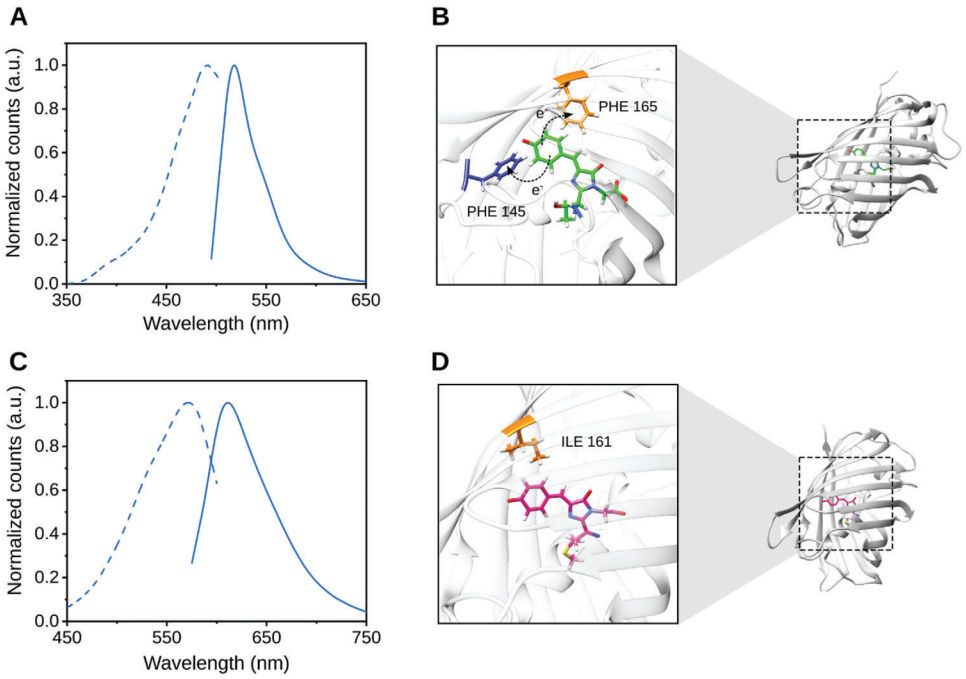

Figure 4. A) Excitation (dashed line) and emission (solid line) of FTO/TiO_2/hybrid-sfGFP. B) Electron acceptor residues at less than 4 Å from the chromophore in sfGFP. C) Excitation (dashed line) and emission (solid line) of FTO/TiO_2/hybrid-mCherry. D) Electron acceptor residues at less than 4 Å from the chromophore in mCherry.

adsorption onto TiO_2 electrodes or an effective charge transfer process from the excited hybrid sfGFP to the conduction band of the TiO_2 electrode. The earlier is not supported by the similar emission and excitation spectra shape of the electrodes compared to those of reference films and solution – Figure 3E,F. Thus, we recall the photo-induced oxidation reactions in GFP derivatives have been shown in solution[23,37,38] and application in cell bio-imaging.[39–41] Here, the aromatic tryptophan, tyrosine, or phenylalanine amino acids located at the immediate vicinity of their chromophore (< 4 Å) enable a carrier hopping mechanism.[42,43] In sfGFP, two phenylalanines (PHE145 and PHE165) are adjacent to the chromophore at 2.28 and 3.92 Å, respectively. Thus, they can act as initial electron acceptors for two-step-mediated electron transfer pathways toward the conduction band of the metal oxide electrodes – Figure 4B. First support on this statement comes from the similar τ and ϕ values found in FTO/TiO_2 or SiO_2/hybrid-mCherry films – vide supra, since this protein does not feature any photo-induced redox behavior in solution as no aromatic amino acids near its chromophore are present – Figure 4D.[23,37–41]

To further validate our hypothesis, three additional experiments were carried out. At first, the electron-accepting features of both hybrid FPs were studied in p-type FTO/NiO electrodes. In line with the above results, the emission/excitation spectra **– Figure** 5A,C – and the photoluminescence figures are similar to those of reference sensitized SiO_2 films –, i.e., 2.3 ns / 51% and 1.5 ns / 23% for FTO/NiO/hybrid-sfGFP and -mCherry, respectively, indicating that both hybrids are not photo-induced acceptors.[22] Second, the photo-induced electron transfer process from the hybrid sfGFPs to TiO_2 electrode was studied in FTO/TiO_2/SiO_2/hybrid-sfGFP, promoting the formation of a very thin SiO_2 dielectric interlayer (< 1 nm, *ca.* 5, 15, and 25 nm) onto the TiO_2 electrode by spin coating TEOS solution prior sensitization with the hybrid FP – see supporting information. As shown by atomic force microscopy (AFM), the mesoporous morphology of the TiO_2 electrodes is preserved for interlayers of a few nm, while it became less rough with thicker SiO_2 interlayers – Figure S3 (Supporting Information). The use of very thin interlayers (<5 nm) leads to a three-fold increase of the hybrid sfGFP uptake – Figure S4 (Supporting Information) – and a further reduction of τ and ϕ values to <1.3 ns and <25%. In addition, these electrodes feature a remarkable stable photoluminescence features over 6 months under storage conditions – Figure 5B,D. This is in perfect agreement with the excellent stability of the reference films attributed to the formation of the partial ion silica shell around the FPs – vide supra. Finally, thick interlayers reduce the mesoporosity of the electrodes, reducing the FP uptake – Figures S3 and S4 (Supporting Information) –, and act as an electron transfer barrier, increasing the τ and ϕ values to those noted for reference FTO/SiO_2/hybrid-sfGFP films –, i.e., 1.82 ns/ 45% and 2.04 ns/ 46% for FTO/TiO_2/SiO_2(15 and 25 nm)/hybrid-sfGFP films versus 2.48 ns / 52% for FTO/SiO_2/hybrid-sfGFP films.

As third and final experiment, the electron transfer mechanism from sfGFP to the TiO_2 electrode was controlled by simple single point mutations of the aromatic amino acids nearest to the chromophore by residues with higher or none reducing potential. Due to the higher structural conservation of PHE165 across the fully characterized GFP-like fluorescent proteins lineages – Figure S5A (Supporting Information), we preferentially targeted the pathway at position 145, mutating PHE either to a stronger electron acceptor Tyrosine (TYR)[44] or

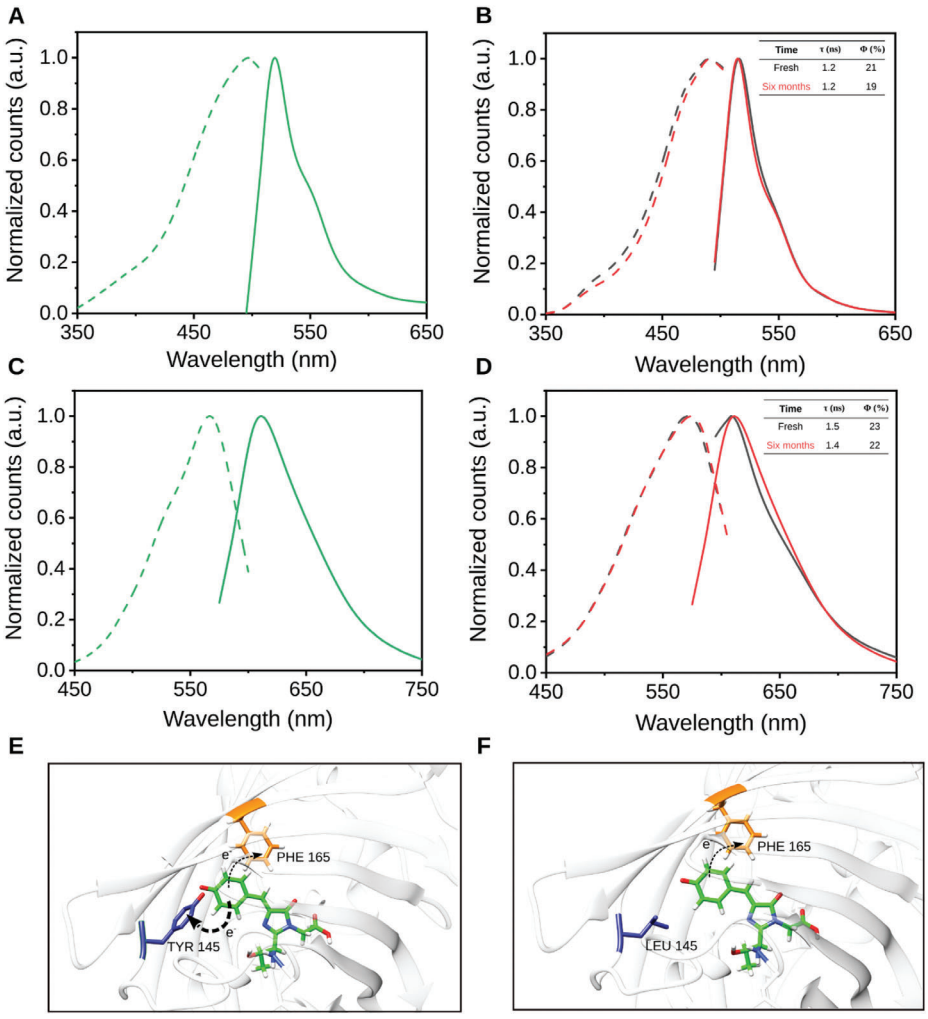

Figure 5. A) Excitation (dashed line) and emission (solid line) of FTO/NiO/hybrid-sfGFP (green). B) Excitation (dashed line) and emission (solid line) spectra and their respective figures-of-merit gathered in the table of fresh (black) and 6 months-old (red) FTO/TiO_2/SiO_2/hybrid-sfGFP. C) Excitation (dashed line) and emission (solid line) of FTO/NiO/hybrid-mCherry (green). D) Excitation (dashed line) and emission (solid line) spectra and their respective figures-of-merit gathered in the table of fresh (black) and 6 months-old (red) FTO/TiO_2/SiO_2/hybrid-mCherry. Electron acceptor residues at less than 4 Å from the chromophore in sfGFP-TYR145 E) and sfGFP-LEU145 F). *All τ fittings and ϕ gave errors <0.03 and <2% respectively.

to a poor acceptor Leucine (LEU)[45] – Figure 5E,F. The presence of TYR145 is directly reflected on sfGFP's photoluminescence figures in solution, showing the same emission band shape – Figure S5B,C (Supporting Information) –, but with a decrease in both τ –, i.e., 2.7 ns – and a two-fold quicker photobleaching (450 nm; 95 mW cm^2) in the presence of acceptor species in solution compared to native sfGFP – Figure S5D (Supporting Information). While the mutation to LEU145 leads to enhanced τ –, i.e., 3.3 ns – and a 1.5-fold enhanced photostability in the presence of acceptor species in solution compared to sfGFP – Figure S5D (Supporting Information). In other words, the photo-induced electron donor capacity goes from sfGFP-TYR145 to native sfGFP and finally to sfGFP-LEU145. This trend is also nicely reflected in the FTO/TiO_2/SiO_2(5 nm) sensitized with their above respective hybrids. In short, the electrodes with sfGFP-TYR145 featured the same emission band with a strong reduction of the τ and ϕ compared to the same films with native sfGFP (*i.e.*, 0.9 ns vs 1.3 ns and 6.2% vs 25%), while those with sfGFP-LEU145 showed an increase of τ and ϕ up to 1.8 ns and 32%.

In light of these findings, we conclude that i) the hybrid sfGFPs can act as an efficient and stable electron donor photosensitizer coupled with TiO_2 electrodes and ii) the photo-induced electron transfer hopping mechanism is mediated by the aromatic amino acids placed at positions 145 and 165, being the most relevant the electron transfer pathway via the position 145 that is located at the initial loop of the strand β7 and, in turn, it is more exposed to the outside surrounding of the FP – Figure 5.

2.3. Optimization of Bio-DSSCs with Hybrid FPs

The optimization of the bio-DSSCs was achieved by combining FTO/TiO_2 (12 µm)/SiO_2 (0 and <5 nm)/hybrid-sfGFP photoan-

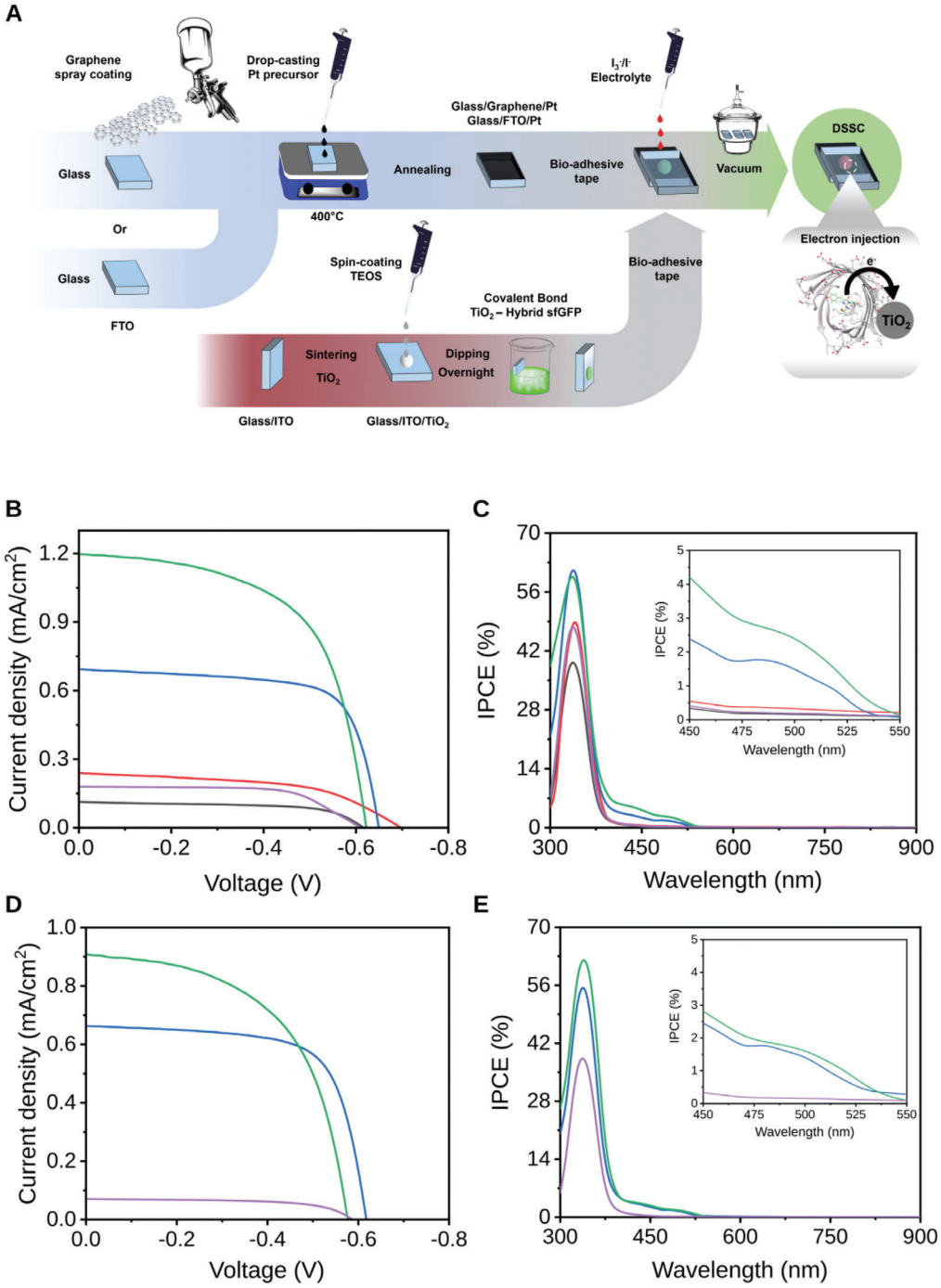

Figure 6. A) Step-to-step fabrication method of bio-DSSCs with hybrid FPs. J-V curve B) under 1 sun AM 1.5 conditions and IPCE C) of TiO_2/hybrid sfGFP/ACN/Pt (black), TiO_2/SiO_2/hybrid sfGFP-F145L/MCN/Pt (violet), TiO_2/hybrid sfGFP/MCN/Pt (red), TiO_2/SiO_2/hybrid sfGFP/MCN/Pt (blue), TiO_2/SiO_2/hybrid sfGFP-F145Y/MCN/Pt (green). *J–V* curve D) under 1 sun AM 1.5 conditions and IPCE E) of TiO_2/SiO_2/hybrid sfGFP-F145L/MCN/Pt-Gr (violet), TiO_2/SiO_2/hybrid sfGFP/MCN/Pt-Gr (blue), TiO_2/SiO_2/hybrid sfGFP-F145Y/MCN/Pt-Gr (green).

odes with either Pt/FTO or Pt/graphene/glass counter electrodes using different solvent-based electrolytes along with reference devices without hybrid sfGFP – see supporting information. Step-to-step fabrication methodology, current-voltage (*J–V*) curves, and incident-photon-to-current conversion efficiency (IPCE) spectra are shown in **Figure 6**, while the performance of the most representative devices is gathered in **Table 1**.

At first, the standard bio-DSSC architecture –, i.e., acetonitrile (ACN) based electrolyte and Pt/FTO counter-electrode,[20,24] – and the native sfGFP hybrid were applied to devices with both photoanodes – see Supporting Information. Unfortunately, the sensitized photoanodes FTO/TiO_2/SiO_2/hybrid-sfGFP were

Table 1. Device performance of the most representative sfGFP-based bio-DSSCs.

	V_{OC} [mV]	J_{SC} [mA cm^{-2}]	FF [%]	η [%]
Pt				
TiO_2/hybrid sfGFP/ACN/Pt	620	0.11	61	0.04
TiO_2/hybrid sfGFP/MCN/Pt	701	0.24	52	0.09
TiO_2/SiO_2/hybrid sfGFP/MCN/Pt	650	0.69	70	0.32
TiO_2/SiO_2/hybrid sfGFP-F145Y/MCN/Pt	625	1.21	60	0.45
TiO_2/SiO_2/hybrid sfGFP-F145L/MCN/Pt	613	0.18	64	0.08
Pt-Gr				
TiO_2/SiO_2/hybrid sfGFP/MCN/Pt-Gr	620	0.66	63	0.26
TiO_2/SiO_2/hybrid sfGFP-F145Y/MCN/Pt-Gr	581	0.91	56	0.30
TiO_2/SiO_2/hybrid sfGFP-F145L/MCN/Pt-Gr	591	0.07	56	0.02

quickly photo-bleached in contact with this electrolyte – Figure S6 (Supporting Information), leading to state-of-the-art device stabilities of a few seconds/minutes.[19–22] Indeed, the devices showed a similar performance to that of reference devices with bare TiO_2 photoanodes – Figure S6 and Table S1 (Supporting Information), while the IPCE spectra is featureless in the 450–550 nm region, confirming the lack of the electron transfer from the hybrid sfGFP to the TiO_2. This might be related to the protonation of the chromophore upon contact with the ACN electrolyte as shown in Figure S7 (Supporting Information).

Among the family of organic nitrile solvents, we selected the low-volatile and highly bio-compatible methoxypropionitrile (MCN) organic solvent.[46] In detail, a mixture of MCN:H_2O at different volume ratios (100:0 and 80:20) was studied in concert with iodide/triiodide redox pairs. As shown in Figure 5B and Figure S8 (Supporting Information), the FTO/TiO_2/SiO_2/hybrid-sfGFP photo-anodes exposed to MCN-based electrolytes were stable over months, leading to a 2-fold increase of the J_{sc} (240 µA cm^{-2}) and slightly enhanced V_{oc} (0.701 V) compared to reference bare TiO_2 devices – Table 1. This goes hand-in-hand with the contribution of FP sensitizer in the IPCE – Figure S8 (Supporting Information). Unfortunately, the J_{sc} and the FP contribution at the IPCE is significantly reduced using a 80:20 electrolyte due to the hydrophobic nature of TiO_2 that might hamper regeneration processes.[47] Although photocurrent is not high, MCN-based electrolyte assurance device stability and, in turn, this represents the best option to develop highly performing bio-DSSCs.

In this rationale line, bio-DSSCs were fabricated by combining i) the best FTO/TiO_2/SiO_2(5 nm) photo-anode, which showed a higher FP loading (three-fold) and enhanced charge injection – vide supra, ii) the three sfGFP hybrid variants to corroborate the electron transfer mechanism in solar cells, and iii) Pt/FTO and Pt/graphene/glass electrodes with the above MCN-based electrolyte to show the versatility of our approach – Figure 6 and Table 1. Regardless of the type of counter-electrode, devices with native sfGFP hybrid featured a strongly increased J_{sc} up to 660 µA cm^{-2} – Figure 6. This goes hand-in-hand with *ca.* 3-fold intensity increase in both the absorption features of the electrode and the IPCE response at the 450–550 nm region compared to those of devices with FTO/TiO_2/SiO_2/hybrid-sfGFP – Figures S4 and S8 (Supporting Information), while those with ACN-based electrolyte were featureless as the reference bare TiO_2 devices – Figure 6. These findings confirm the electron injection from the hybrid sfGFP to TiO_2 upon direct excitation. As expected, the J_{sc} improvement is also associated with an increase of the FF from 52% to 70% – Table 1, as the TEOS addition also acts as a protective layer of the FTO, reducing undesired electron-back transfer process at both FTO/electrolyte and FTO/TiO_2/electrolyte interfaces. Overall, these figures led to an increase of η up to state-of-the-art values of 0.3% – Table 1.[20]

In line with the above spectroscopic studies, devices with the variant sfGFP-LEU145 hybrid exhibited a very poor J_{sc} of 0.18 mA cm^2 associated with a low IPCE contribution, as the electron transfer pathway via position 165 is unfavorable – Figure 6. As expected from the τ and ϕ changes in films – vide supra, devices with the variant sfGFP-TYR145 hybrid featured a two-fold enhancement of the J_{sc} and IPCE contribution compared to those with native sfGFP hybrid – Table 1 and Figure 6. Indeed, the photogenerated current of 1.2 mA cm^{-2} represents a record in FP-based bio-DSSCs.[19–22] This goes hand-in-hand with a similar Voc and FF values that lead to an efficiency value of 0.6% that is the most efficient bio-DSSCs with biogenic photo-sensitizers (0.18%),[18] in general, and the most efficient protein-based solar cells to date (0.35%),[20] in particular. As a

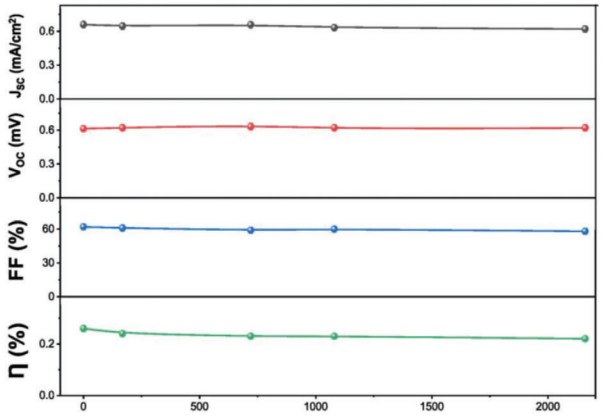

Device parameter	Fresh	> 2000 hrs
J_{SC} (mA/cm²)	0.66	0.62
V_{OC} (mV)	613	620
FF (%)	62	58
η (%)	0.26	0.22

Figure 7. Figures-of-merit of sfGFP-based bio-DSSCs over time.

final remark, the device stability under 1 sun AM1.5 illumination was studied (**Figure 7**). In short, figures-of-merit of devices with sfGFP-TYR145 hybrid gradually reduced, reaching their half values after 300 h, while those with native sfGFP hybrid were stable (<5% loss). Spectroscopic analysis of the sensitized electrodes indicates that the chromophore is deactivated via H-transfer process to its inert neutral form. Indeed, the above described photobleaching studies in solution also confirmed that this variant sfGFP-TYR145 is 2-fold less stable than the native one – Figure S5D (Supporting Information). What is more striking, the device with the native sfGFP hybrid was fully operative with a <10% loss after 2,200 h (90 days; Figure 7), truly attesting to the success of using hybrid FPs photosensitizers in solar energy conversion schemes as the most stable biogenic photosensitizer led to device stabilities of <200 h at 0.18%.[18]

3. Conclusion

This work sets in a successful strategy to exploit the photo-induced electron donor features of fluorescent proteins in solar cell schemes. This requires a straightforward chemical functionalization with alkoxysilane groups that leads to hybrid FPs with i) enhanced stabilities over six months in both aqueous solutions and foreign environments, such as organic solvent-based electrolytes and sensitized dry n-/p-type metal oxide films, ii) easy adsorption and enhanced uptake (three-fold) on n-/p-type metal oxide films, allowing to study and optimize their electron donor and acceptor features, and iii) outstanding solar cell figures-of-merit compared to the prior-art FP-sensitizer based devices. Here, the optimized device configuration using our hybrid FPs (TiO_2/SiO_2(<5 nm)/hybrid-sfGFP/MCN-electrolyte/Pt-FTO/graphene) results in J_{sc} of 660 µA cm^{-2}, V_{oc} of 0.66 V, FF of 70%, and η of 0.3% that are stable >2,000 h, outperforming both, the prior-art stability (a few seconds/minutes) of FP-based solar cells and bio-DSSCs with biogenic donor materials (curcumin dyes; < 200 h at η of 0.18%). Overall, this work provides a successful concept that could be applied to any photo/redox protein, enabling further advances in the implementation and stability of FP-based photosensitizers for solar-energy driven technologies, in general, and bio-hybrid solar cells, in particular.

Supporting Information

Supporting Information is available from the Wiley Online Library or from the author.

Acknowledgements

S.W., M.N., and M.P. contributed equally to this work. R.D.C., M.P., and D.G.-A. acknowledge the European Union's Horizon 2020 research and innovation ERC-Co InOutBioLight No. 816856. M.N. and R.D.C. acknowledge FPNP-BioLED No. 101022975 funded by H2020-MSCA-IF-2020 of the European Commission. S.C., L.M.C., M.G.-Ll, S.L., and R.D.C. acknowledge STiBNite No. 956923 funded by H2020-MSCA-ITN-2020 of the European Commission.

Open access funding enabled and organized by Projekt DEAL.

Conflict of Interest

The authors declare no conflict of interest.

Data Availability Statement

The data that support the findings of this study are available from the corresponding author upon reasonable request.

Keywords

biogenic electron donors, bio-optoelectronics, bio-hybrid solar cells, hybrid fluorescent proteins, stability

Received: November 16, 2023
Revised: December 30, 2023
Published online: January 26, 2024

[1] N. Lämmermann, F. Schmid-Michels, A. Weißmann, L. Wobbe, A. Hütten, O. Kruse, *Sci. Rep.* **2019**, *9*, 2109.
[2] M. I. Ortiz-Torres, M. Fernández-Niño, J. C. Cruz, A. Capasso, F. Matteocci, E. J. Patiño, Y. Hernández, A. F. González Barrios, *Sci. Rep.* **2020**, *10*, 3376.
[3] C. C. Villarreal, S. Monge, D. Aguilar, A. Tames, N. Araya, M. Aguilar, S. Ramakrishna, V. Thavasi, Z. Song, A. Mulchandani, R. Venkatesan, *Mater. Today Energy* **2022**, *23*, 100910.
[4] L. M. Cavinato, E. Fresta, S. Ferrera, R. D. Costa, *Adv. Energy. Mater* **2021**, *11*, 2100520.
[5] M. L. Chávez-González, L. Sepúlveda, D. K. Verma, H. A. Luna-García, L. V. Rodríguez-Durán, A. Ilina, C. N. Aguilar, *Processes* **2020**, *8*, 434.
[6] Y. Hou, K. Wang, D. Yang, Y. Jiang, N. Yennawar, K. Wang, M. Sanghadasa, C. Wu, S. Priya, *ACS Energy Lett.* **2019**, *4*, 2646.
[7] X. F. Wang, A. Matsuda, Y. Koyama, H. Nagae, S. Ichi Sasaki, H. Tamiaki, Y. Wada, *Chem. Phys. Lett.* **2006**, *423*, 470.
[8] S. Das, C. Wu, Z. Song, Y. Hou, R. Koch, P. Somasundaran, S. Priya, B. Barbiellini, R. Venkatesan, *ACS Appl. Mater. Interfaces* **2019**, *11*, 30728.
[9] K. Yao, H. Jiao, Y. X. Xu, Q. He, F. Li, X. Wang, *J. Mater. Chem. A* **2016**, *4*, 13400.
[10] S. Lizin, S. Van Passel, E. De Schepper, W. Maes, L. Lutsen, J. Manca, D. Vanderzande, *Energy Environ. Sci.* **2013**, *6*, 3136.
[11] M. D. M. Faure, B. H. Lessard, *J. Mater. Chem. C* **2021**, *9*, 14.
[12] C. Barbec, H. J. Egelhaaf, M. Salvador, *J. Mater. Res.* **2018**, *33*, 1839.
[13] M. Irimia-Vladu, *Chem. Soc. Rev.* **2014**, *43*, 588.
[14] Y. C. Shih, Y. B. Lan, C. S. Li, H. C. Shih, L. Wang, I. C. Wu, K. F. Lin, *Small* **2017**, *13*, 1604305.
[15] J. Huang, K. X. Wang, J. J. Chang, Y. Y. Jiang, Q. S. Xiao, Y. Li, *J. Mater. Chem. A* **2017**, *5*, 13817.
[16] F. Bella, D. Pugliese, L. Zolin, C. Gerbaldi, *Electrochim. Acta* **2017**, *237*, 87.
[17] K. T. Huang, C. P. Chen, B. H. Jiang, R. J. Jeng, W. C. Chen, *Org. Electron.* **2020**, *87*, 105924.
[18] Y. V. A. Suyitno, L. L. G. Hidajat, B. Kristiawan, A. H. Wibowo, *Int. Energy J.* **2018**, *18*, 53.
[19] H. A. Maddah, V. Berry, S. K. Behura, *Renewable Sustainable Energy Rev.* **2020**, *121*, 109678.
[20] R. Mohammadpour, S. Janfaza, M. Zeinoddini, *Biomass Bioenergy* **2016**, *87*, 35.
[21] R. Mohammadpour, S. Janfaza, *ACS Sustainable Chem. Eng.* **2015**, *3*, 809.
[22] A. Acharya, A. M. Bogdanov, B. L. Grigorenko, K. B. Bravaya, A. V. Nemukhin, K. A. Lukyanov, A. I. Krylov, *Chem. Rev.* **2017**, *117*, 758.
[23] A. M. Bogdanov, A. S. Mishin, I. V. Yampolsky, V. V. Belousov, D. M. Chudakov, F. V. Subach, V. V. Verkhusha, S. Lukyanov, K. A. Lukyanov, *Nat. Chem. Biol.* **2009**, *5*, 459.

[24] K. Deepankumar, A. George, G. K. Priya, M. Ilamaran, N. R. Kamini, T. S. Senthil, S. Easwaramoorthi, N. Ayyadurai, *ACS Sustainable Chem. Eng.* **2017**, *5*, 72.
[25] V. Bolis, C. Busco, M. Ciarletta, C. Distasi, J. Erriquez, I. Fenoglio, S. Livraghi, S. Morel, *J. Colloid Interface Sci.* **2012**, *369*, 28.
[26] F. Hoffmann, M. Fröba, *Chem. Soc. Rev.* **2011**, *40*, 608.
[27] S. Sfameni, T. Lawnick, G. Rando, A. Visco, T. Textor, M. R. Plutino, *Nanomaterials* **2022**, *9*, 3404.
[28] D. Meroni, L. L. Presti, G. Di Liberto, M. Ceotto, R. G. Acres, K. C. Prince, R. Bellani, G. Soliveri, S. Ardizzone, *J. Phys. Chem. C* **2017**, *121*, 430.
[29] P. Rokicka-Konieczna, A. Wanag, A. Sienkiewicz, E. Kusiak-Nejman, A. W. Morawski, *Catal. Commun.* **2020**, *134*, 105862.
[30] K. M. Dean, J. L. Lubbeck, J. K. Binder, L. R. Schwall, R. Jimenez, A. E. Palmer, *Biophys. J.* **2011**, *101*, 961.
[31] N. V. Visser, J. W. Borst, M. A. Hink, A. Van Hoek, A. J. W. G. Visser, *Biophys. Chem.* **2005**, *116*, 207.
[32] G. Donnert, C. Eggeling, S. W. Hell, *Nat. Methods* **2007**, *4*, 81.
[33] A. B. T. Ghisaidoobe, S. J. Chung, *Int. J. Mol. Sci.* **2014**, *15*, 22518.
[34] S. Feihl, R. D. Costa, W. Brenner, J. T. Margraf, R. Casillas, O. Langmar, A. Browa, T. E. Shubina, T. Clark, N. Jux, D. M. Guldi, *Chem. Commun.* **2014**, *50*, 11339.
[35] F. Lodermeyer, R. D. Costa, R. Casillas, F. T. U. Kohler, P. Wasserscheid, M. Prato, D. M. Guldi, *Energy Environ. Sci.* **2015**, *8*, 241.
[36] J. Hongmei, Z. Zhen, L. Zhiming, W. Xinling, *Ind. Eng. Chem. Res.* **2006**, *45*, 8617.
[37] B. L. Grigorenko, A. V. Nemukhin, D. I. Morozov, I. V. Polyakov, K. B. Bravaya, A. I. Krylov, *J. Chem. Theory Comput.* **2012**, *8*, 1912.
[38] J. J. Van Thor, T. Gensch, K. J. Hellingwerf, L. N. Johnson, *Nat. Struct. Mol. Biol.* **2002**, *9*, 37.
[39] K. A. Lukyanov, V. V. Belousov, *Biochim. Biophys. Acta, – Gen. Subj.* **2014**, *1840*, 745.
[40] D. M. Shcherbakova, V. V. Verkhusha, *Curr. Opin. Chem. Biol.* **2014**, *20*, 60.
[41] D. M. Chudakov, M. V. Matz, S. Lukyanov, K. A. Lukyanov, *Physiol. Rev.* **2010**, *90*, 1103.
[42] Y. Tan, R. Y. Adhikari, N. S. Malvankar, S. Pi, J. E. Ward, T. L. Woodard, K. P. Nevin, Q. Xia, M. T. Tuominen, D. R. Lovley, *Small* **2016**, *12*, 4481.
[43] N. L. Ing, M. Y. El-Naggar, A. I. Hochbaum, *J. Phys. Chem. B* **2018**, *122*, 10403.
[44] A. M. Bogdanov, A. Acharya, A. V. Titelmayer, A. V. Mamontova, K. B. Bravaya, A. B. Kolomeisky, K. A. Lukyanov, A. I. Krylov, *J. Am. Chem. Soc.* **2016**, *138*, 4807.
[45] R. C. G. Creasey, A. B. Mostert, A. Solemanifar, T. A. H. Nguyen, B. Virdis, S. Freguia, B. Laycock, *ACS Omega* **2019**, *4*, 1748.
[46] S. Venkatesh, S. C. Su, S. C. Kao, H. Teng, Y. L. Lee, *J. Power Sources* **2015**, *274*, 506.
[47] F. Bella, C. Gerbaldi, C. Barolo, M. Grätzel, *Chem. Soc. Rev.* **2015**, *44*, 3431.